Mirdrikvand, Mojtaba and Ridder, Harm and Thöming, Jorg and Dreher, Wolfgang

Diffusion weighted magnetic resonance imaging for temperature measurements in catalyst supports with an axial gas flow

Journal Article	as:	peer-reviewed accepted version (Postprint)
DOI of this document*(secondary publication):		https://doi.org/10.26092/elib/2475
Publication date of this document:		22/09/2023

* for better findability or for reliable citation

Recommended Citation (primary publication/Version of Record) incl. DOI:

Mirdrikvand, Mojtaba and Ridder, Harm and Thöming, Jorg and Dreher, Wolfgang,
Diffusion weighted magnetic resonance imaging for temperature measurements in catalyst supports with an axial gas flow
React. Chem. Eng., 2019, 4, 10, 1844-1853, The Royal Society of Chemistry
http://dx.doi.org/10.1039/C9RE00082H

Diffusion weighted magnetic resonance imaging for temperature measurements in catalyst supports with an axial gas flow†

Mojtaba Mirdrikvand, *[a] Harm Ridder,[b] Jorg Thöming [b] and Wolfgang Dreher [a]

In situ thermometry of catalytic gas phase reactions allows the determination of temperature profiles in catalyst beds. In NMR imaging systems used for measuring the chemical composition of species in model reactors, temperature measurements by NMR spectroscopy are technically challenging and confined to a rather low temperature range. In this study, an optimized NMR *in situ* technique is proposed, which will allow the determination of the temperature distribution in highly exothermic reactions on structured catalysts. Diffusion weighted magnetic resonance imaging (DW-MRI) was successfully applied as an alternative method for temperature measurements commonly performed by chemical shift measurements using ethylene glycol. DW-MRI applied with different diffusion sensitizing gradients allows high-resolution imaging of the temperature dependent diffusion coefficient, without the need for high spatial homogeneity of the magnetic field. Using 3D DW-MRI on ethylene glycol, glycerol, and the temperature stable ionic liquid Pyr_{13}[TFSI] (decomposition temperature of 400 °C) as NMR thermometers, measurements were performed in a temperature range from 20 to 160 °C. The proposed method can be used in reaction engineering approaches performed in NMR systems.

Received 22nd February 2019,
Accepted 24th July 2019

DOI: 10.1039/c9re00082h

1. Introduction

In the chemical industry, a large number of processes include reactions driven by heterogeneous catalysts. Heterogeneous catalysts are consistently involved with complex gas–solid or liquid–solid interfaces that occur in pores and channels of the catalyst supports. This complex nature leads to an uneven distribution of temperature and composition in exothermic reaction systems such as the Sabatier process, Fischer–Tropsch synthesis or hydrogenation reactions.[1,2] Therefore, proper *in situ* characterization methods are of great interest to extract vital information from these processes and to validate numerical simulations at the micro- and macro-scale. The latter helps to achieve higher process efficiency and reduced industrial costs and to predict possible risks in large-scale reactors. In particular, measuring temperature profiles in the radial and axial directions of a reactor filled with catalysts helps to better understand the variation of temperature in the catalyst body, define realistic values for boundary conditions in numerical simulations, and reduce the threat of thermal runaway by predicting the formation of hot spots in reactors.

Different techniques have been applied to measure the temperature of monolithic catalysts under reaction conditions. Conventional tracers give limited point-wise information about the temperature by inserting thermocouples through the catalyst body.[3] Unlike conventional methods, other *in situ* techniques including infrared thermography, near-infrared diffuse transmittance tomography, and X-ray diffraction (XRD) are non-invasive and the use of them has grown tremendously in recent years.[4–7] However, all these methods have certain limitations, especially when an opaque reactor is studied.[8–11] Nuclear magnetic resonance (NMR) methods are another well-known non-destructive approach for the quantitative characterization of transport processes and chemical reactions in chemical engineering. NMR is even more advantageous when a spatially resolved study of opaque reactors is performed. Moreover, NMR allows measurements of many different process characteristics such as temperature, velocity, diffusion and composition of species under identical reaction conditions.

NMR thermometry is based on the measurement of indirect parameters such as chemical shift differences, relaxation times of longitudinal magnetization, self-diffusion coefficients, and signal intensities. All these parameters can affect the NMR signal in case of a variation in temperature.

Among the aforementioned approaches, localized NMR spectroscopy and magnetic resonance spectroscopic imaging (MRSI) are most often the methods of choice to analyze the

[a] *The University of Bremen, Department of Chemistry, In vivo MR group, Leobener Str. 7, 28359 Bremen, Germany. E-mail: Mirdrikvand@uni-bremen.de*

[b] *The University of Bremen, Center for Environmental Research and Sustainable Technology (UFT), Leobener Str. 6, 28359 Bremen, Germany*

† Electronic supplementary information (ESI) available. See DOI: 10.1039/c9re00082h

temperature of the catalyst bed in reaction engineering approaches.[8,12–15] To perform these experiments, very thin glass-made capillaries or capsules, referred to as "NMR thermometers", are filled with a probing liquid. In each volume element (voxel), the chemical shift difference between different spectral peaks of the probing liquid is determined. The temperature can be measured using the known relation between temperature and the chemical shift difference between two peaks. Therefore, the method does not depend on an external reference.

In reaction engineering, ethylene glycol has been used as a temperature probe in catalyst supports, measuring the chemical shift difference between the OH and the CH_2 signals.[8,14–16] It could be shown that the measurements were in very good agreement with simulations of temperature profiles in a heterogeneous catalytic reaction.[17] However, the applicability of this approach is limited by the liquid's boiling point (197.3 °C at ambient pressure) and the limited separation of both signals caused by the decreasing chemical shift difference with increasing temperature. Additionally, MRSI highly depends on the spatial homogeneity of the static magnetic field, which limits the applicability of the method at elevated temperatures, where the spectral peaks overlap one another and hamper accurate temperature measurements. Thus, only temperatures up to 150–160 °C can be measured by the MRSI of ethylene glycol.

Therefore, an alternative method is essential to extend the temperature range and overcome the need for high field homogeneity. For biomedical MRI, several techniques have been proposed for temperature mapping. In particular, the temperature dependence of the chemical shift, the diffusion coefficient or the spin–lattice relaxation time T_1 of water has been exploited for spatially resolved temperature measurements in humans and animals.[18–22] Since diffusion weighted MRI (DW-MRI) has found widespread use in biomedical and clinical MRI,[20,23] numerous fast DW-MRI pulse sequences have been developed.[24] Hence, DW-MRI can be a solution for temperature measurements in an extended temperature range using NMR thermometers filled with liquids exhibiting high boiling points, such as glycerol (boiling temperature of 289 °C) or ionic liquids (chemical decomposition at temperatures above 400 °C).

The aim of this work is to support the hypothesis that DW-MRI can be used as a tool for determining temperatures in broad and high temperature ranges. Since DW-MRI is more robust against magnetic field inhomogeneities as compared to MRSI, temperature measurements by DW-MRI might also be an interesting alternative for temperature ranges in which MRSI of ethylene glycol can be applied. A comparison of MRSI and DW-MRI, which displays the dependency of MRSI on field inhomogeneities, is included in the ESI.† An optimized DW-MRI sequence was applied to measure the diffusion coefficient and, thus, the temperature using three NMR thermometers filled with ethylene glycol, glycerol or the ionic liquid Pyr_{13} [TFSI]. MRSI of ethylene glycol was used for comparison. Furthermore, fiber optical temperature sensors were placed in the reactor, allowing an estimation of the temperature stability during the measurements. Optimized 3D DW-MRI acquires images with a high spatial resolution using different diffusion sensitizing gradients corresponding to different diffusion weightings. The acquired NMR data were analyzed automatically to accelerate the evaluation of the NMR data in a robust and reliable way.

2. Theory and method

The effect of diffusion on the NMR signal amplitude was already recognized in an early publication by Hahn.[25] Stejskal and Tanner proposed accurate diffusion measurements by incorporating a pair of diffusion sensitizing gradients into a spin echo sequence (*cf.*, Fig. 1).[26] Diffusion characterized by the diffusion coefficient D causes the damping of the NMR signal amplitude according to

$$S = S_0 \cdot e^{-b \cdot D} \tag{1}$$

where S and S_0 are the signal amplitudes measured with and without diffusion sensitizing gradients, respectively. The so-called "b-value" b, which determines the strength of diffusion weighting, is given by

$$b = \gamma^2 \cdot G^2 \cdot \delta^2 \cdot \left(\Delta - \frac{\delta}{3} \right) \tag{2}$$

with the gyromagnetic ratio γ, the gradient strength G, the duration δ of each diffusion sensitizing gradient, and the delay Δ between the gradient pulses (*cf.* Fig. 1). The diffusion coefficient D can be determined by fitting the signal intensities, which are measured in at least two scans with different b-values, to eqn (1).

To estimate the temperature dependence of the diffusion coefficient D, different approaches are reported in the literature. For instance, in case of self-diffusion of ethylene glycol, the temperature dependence of the diffusion coefficient can be predicted based on the following equation validated by Mitchell *et al.*:[27]

$$D(T)_{\text{ethylene glycol}} = A_0 \cdot T \cdot \exp\left(-\frac{E_a}{RT} \right), \tag{3}$$

with the pre-exponential factor A_0, the activation energy E_a and the universal gas constant R.

For glycerol, the glass transition temperature of T_0 = −93.15 °C has to be considered, leading to the following relation proposed by Tomlinson:[28]

$$D(T)_{\text{glycerol}} = A_0 \cdot T^{1/2} \cdot \exp\left(-\frac{E_a}{R(T - T_0)} \right). \tag{4}$$

As described by Lesch *et al.*,[35] a similar consideration can be done for temperature stable ionic liquids, where the

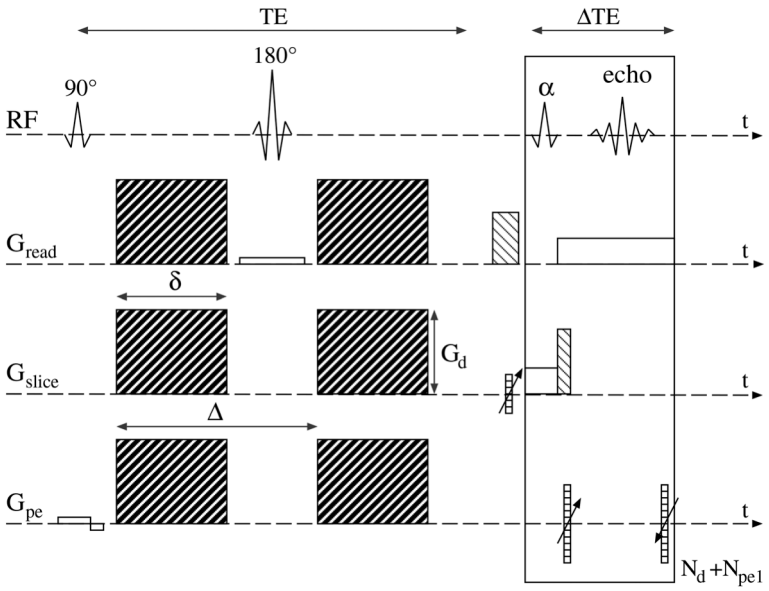

Fig. 1 Scheme of the DW-SE-U-FLARE sequence (not to scale). The four rows display the applied radiofrequency pulses and the detected echo signals as well as the gradient pulses used for diffusion weighting and spatial localization. All acronyms are explained in detail in the text.

diffusion coefficient for the ionic liquid Pyr_{13} [TFSI] can be described by

$$D(T)_{\text{ionic liquid}} = A_0 \cdot \exp\left(-\frac{E_a}{R(T-T_0)}\right), \quad (5)$$

with the glass transition temperature of T_0 = −112.15 °C.

For each liquid, the corresponding diffusion–temperature dependence is used, so the acquired data can be compared over the whole temperature range to the literature data.

Mapping the local diffusion coefficient and consequently the temperature by DW-MRI is of great use in engineering science, *e.g.* for temperature measurements in a model reactor filled with an opaque catalytic material. However, for such applications, the pulse sequence used for DW-MRI has to be chosen carefully. First, a 3D spatial resolution is required to avoid restriction as to the geometry and position of the NMR temperature probes. Second, pulse sequences with a spin echo preparation period should be used to allow diffusion sensitization and avoid signal losses caused by magnetic field inhomogeneities. Third, data acquisition with a multi-echo train will reduce the minimum total measurement time because more spatial encoding steps can be performed per excitation. Fourth, for the echo train, radiofrequency (RF) refocusing should be preferred over gradient refocusing because a rather low B_0 homogeneity and thus short effective transverse relaxation times T_2* are expected for experimental setups such as NMR compatible model reactors.

Following these requirements, a 3D DW-SE-U-FLARE sequence (diffusion weighted spin echo ultrafast low angle rapid acquisition with relaxation enhancement)[29,30] was implemented (*cf.*, Fig. 1). After the 90° excitation pulse, unipolar diffusion sensitizing gradients of strength G_d and duration δ are applied prior to and after the 180° refocusing pulse. Optionally, slice selection gradients can be applied if the object does not fit into the FOV and only a certain part of the object is to be measured (zoom). The diffusion weighted transverse magnetization is refocused with a train of RF pulses with flip angle α. After N_d dummy cycles used to stabilize the echo amplitude, N_{pe1} echoes are acquired under a read gradient, each sampled with different spatial phase encoding using the phase encoding gradient G_{pe}. In N_{pe2} experiments, additional spatial phase encoding is applied prior to the echo train for the spatial resolution in the slice direction. Displaced U-FLARE exploiting only one echo parity was used to avoid image artifacts in case of off-resonance effects.[30]

3. Materials

This section describes the chemicals used as NMR thermometers and the design of the NMR-compatible vessel as a model reactor, which was used for measurements at fixed temperature points.

3.1. Chemicals

Three liquids were investigated as NMR thermometers. Ethylene glycol (≥99.7% purity, VWR International GmbH, Germany) was used as the reference substance. Ethylene glycol was also used for MRSI measurements for comparison with DW-MRI. However, since the rather low boiling point of ethylene glycol limits its fields of application, liquids with higher boiling point or high decomposition temperature are needed. Thus, glycerol (≥99.5% purity, Carl Roth GmbH, Germany) and 1-methyl-3-propylpyrrolidinium bis(trifluoromethylsulfonyl)-imide (Pyr_{13} [TFSI]) (99% purity, ionic liquids technologies (IoLiTec) GmbH, Heilbronn, Germany) were chosen as

alternative NMR thermometers. The choice of the ionic liquid was due to its high decomposition temperature (above 400 °C), which facilitates temperature measurements for a variety of reactions taking place up to this level. The liquids were each filled into capillaries (OD = 0.7 mm, ID = 0.55 mm) made of borosilicate and then sealed by melting the edges.

The capillaries were aligned through the channels of a cordierite honeycomb monolith used as a catalyst support (length: 38 mm, diameter: 25 mm, 600 cells per square inch (cpsi); NGK, Poland). In some experiments, two capillaries were used for each probing liquid to assess the consistency of the measured data for individual capillaries in a thermally homogenous system.

Ambient temperature was used as a starting point. Then, the temperature was increased in different steps. At each step, waiting for a time of approx. 45 minutes was necessary, until the fiber optical thermometer indicated that steady state is achieved. After the steady state was achieved, the NMR measurements were performed as described in section 3.3.

3.2. Model reactor

An NMR compatible model reactor (length: 80 cm, inner diameter: 26 mm) was developed to operate under elevated temperature conditions in the MRI scanner. Pressurized air was heated up and led into the vessel to obtain the desired temperature. It was preferred to use this external heating mechanism over heating by reaction, as each reaction is only applicable in a specific temperature range. Furthermore, possible spatial temperature inhomogeneities due to an inhomogeneous concentration profile can be avoided. The setup was also equipped with a cooling system to prevent damage or detuning of the RF coil. For this purpose, a bank of PTFE tubes, in which a hydrogen-free coolant was circulating, was used. A cryostatic temperature regulator was used to cool the coolant to −5 °C. The air temperature was measured with a resistance thermometer at the inlet of the setup.

In addition to NMR measurements by MRSI and DW-MRI, an MRI compatible gallium arsenide based fiber optic temperature monitoring system (FOTEMP-4, Weidmann Technologies Deutschland GmbH, Dresden, Germany) was used for accurate temperature measurements near the catalyst support. The sensor was placed in the vessel with a 10 cm distance from the honeycomb monolith (*cf.*, Fig. 2). The sensor was primarily used as a safety monitoring element and to check the temperature stability during NMR measurements.

3.3. NMR measurements

A 7 Tesla preclinical NMR imaging system (Biospec 70/20, Bruker Biospin GmbH, Ettlingen, Germany) equipped with a gradient system BGA12S2 (441 mT m^{-1} maximum gradient strength in each direction, 130 μs rise time) was used for all measurements. A quadrature birdcage RF coil (inner diameter of 72 mm) was used for RF excitation and signal detection. The NMR pulse sequences were implemented using the software platform Paravision 5.1.

DW-MRI. SE-DW-U-FLARE was used with the following parameters: FOV = 48 × 48 × 48 mm^3; matrix size of 128 × 64 × 16, slice thickness of 48 mm; 4 averages to increase the SNR with N_d = 5, 6, 7, or 8 to suppress the remaining instabilities of the echo amplitudes; N_{pe1} = 64, interecho delay of 5.3 ms with centered phase encoding in the U-FLARE echo train, N_{pe2} = 16, repetition time TR = 3 s; 90° slice selective refocusing pulse. Different sets of measurements, each with four *b*-values, starting at 50 s mm^{-2} and with an equidistant increment of the applied gradient of Δb = 250, 1000, 2000, 5000, and 15 000 s mm^{-2} were used to account for the large range of diffusion coefficients measured for different liquids at different temperatures. For each set of measurements, only four *b*-values were used in the interest of a short total

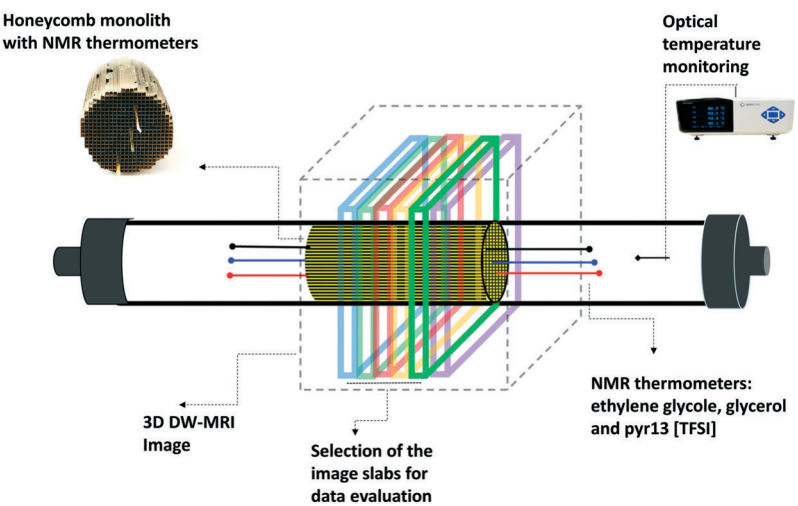

Fig. 2 Scheme of the setup for thermometry using aligned NMR thermometers in the monolith support and an optical temperature monitoring system. 3D DW-MRI enables spatially resolved temperature measurements from the catalyst bed using NMR thermometers. Arbitrary slices can be analyzed from 3D images to determine the temperature.

measurement time. During data processing, the best suited set of *b*-values was used for each combination of liquid and temperature. The measurement time for each scan with four *b*-values was ~13 min.

MRSI. An optimized 3D MRSI pulse sequence was used and the data were evaluated as described in detail in a previous publication.[14] The main experimental parameters were: echo time TE = 350 μs (delay between RF excitation and the start of data acquisition), FOV = 63 × 63 × 126 mm^3, matrix size: 42 × 42 × 42 with spherically reduced *k*-space sampling, repetition time TR = 12.5 ms, and one average yielding a total measurement time of 7 min 32 s.

4. Results and discussion

This section is divided into three main parts. In the first part, the automatic evaluation of DW-MRI images and the procedure to obtain diffusion coefficients are described. In the second part, the results are compared to the literature and theoretical predictions. Finally, we suggest a strategy for the selection of *b*-values to make the measurement procedure more efficient.

4.1. Automatic data analysis

The MRSI data sets were analyzed using an in-house developed IDL (interactive data language, version 7.0, Exelis Visual Information Solutions, Bolder, USA) software program. After apodization with a Hamming function and Fourier transformation along the three spatial directions, the matrix pencil method (MPM)[31] was used to fit the data for the ethylene glycol capillaries. The temperature was determined from the chemical shift values of the two signals detected by the MPM method.[14,16] Since the highest B_0 homogeneity is given in the iso-center of the magnet, the temperatures were determined for three central slices of the ethylene glycol capillaries using the temperature dependent chemical shift differences in the MRSI data. These values were compared to the values determined in the same slices of the 3D DW-MRI data for the three thermometers. No significant temperature differences between the three slices were observed.

The reconstructed DW-MRI images were stored as 32 bit data with the Paravision 5.1 software package. Fig. 3 depicts the generated diffusion weighted images of the thermometers. An in-house developed MATLAB (R2017b, The MathWorks, Inc., Natick, USA) script was used for automated data analysis of the images in order to locate the capillaries in each slice, select the central position and pick the regions of interest (ROIs) for the thermometers. To this end, a noise filter was applied to better visualize the images (*cf.*, Fig. 3) and detect the centers of the capillaries, while the signal intensity of the images stays intact for further evaluations. The images of slices close to the iso-center of the magnet and possessing the lowest *b*-value were used to define the ROIs in each data set for further data analysis. Next, the signal intensities within the selected ROIs were added to obtain a value for the total signal intensity. To further increase the accuracy, the slices located far from the iso-center were also re-analyzed by examining the neighboring slices to ensure that no physical shift of the thermometers has occurred and the central peak of each capillary was correctly chosen. Note that the size of ROIs remains constant for a given capillary during the analysis. For a central slice of the ethylene glycol capillary, the spatial signal distributions around the signal maxima are illustrated in Fig. 4 for four different *b*-values. Note that the four 3D surface plots are uniformly scaled, but the same color map is used in each subfigure for better visibility.

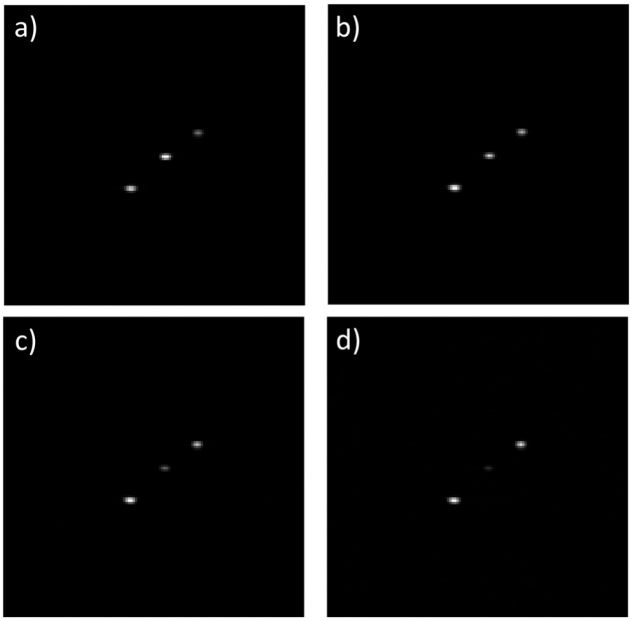

Fig. 3 Diffusion weighted images for the three NMR thermometers filled with ionic liquid Pyr_{13} [TFSI] (top right), ethylene glycol (middle) and glycerol (bottom left) measured at a temperature of 78 °C. The images were measured with different diffusion weightings using *b*-values of 50, 2050, 4050, and 6050 s mm^{-2} (Δb = 2000 s mm^{-2}) for a–d, respectively. Note that the differences in signal intensity correspond to the different diffusion coefficients of the three liquids. The signal intensities are plotted *versus* *b*-values in Fig. 5.

Finally, the temperature dependent diffusion coefficients were estimated for each capillary by fitting the signal intensities determined for different *b*-values to eqn (1).

4.2. Diffusion coefficients

In this section, the diffusion coefficients measured at different temperatures are shown and compared to the literature data. After the thermal steady state was achieved and prior to the DW-MRI measurements, the temperature values were measured by MRSI of ethylene glycol with a standard deviation of ~1.5 °C.

4.2.1. Ethylene glycol. The measured diffusion coefficients for the ethylene glycol thermometers and the literature values[27,32] are plotted in Fig. 6a. The curve predicted by Mitchell *et al.* based on theoretical assumptions[27] (eqn (3)) is also superimposed as a theoretical curve. The diffusion coefficients observed in the current study are in strong agreement

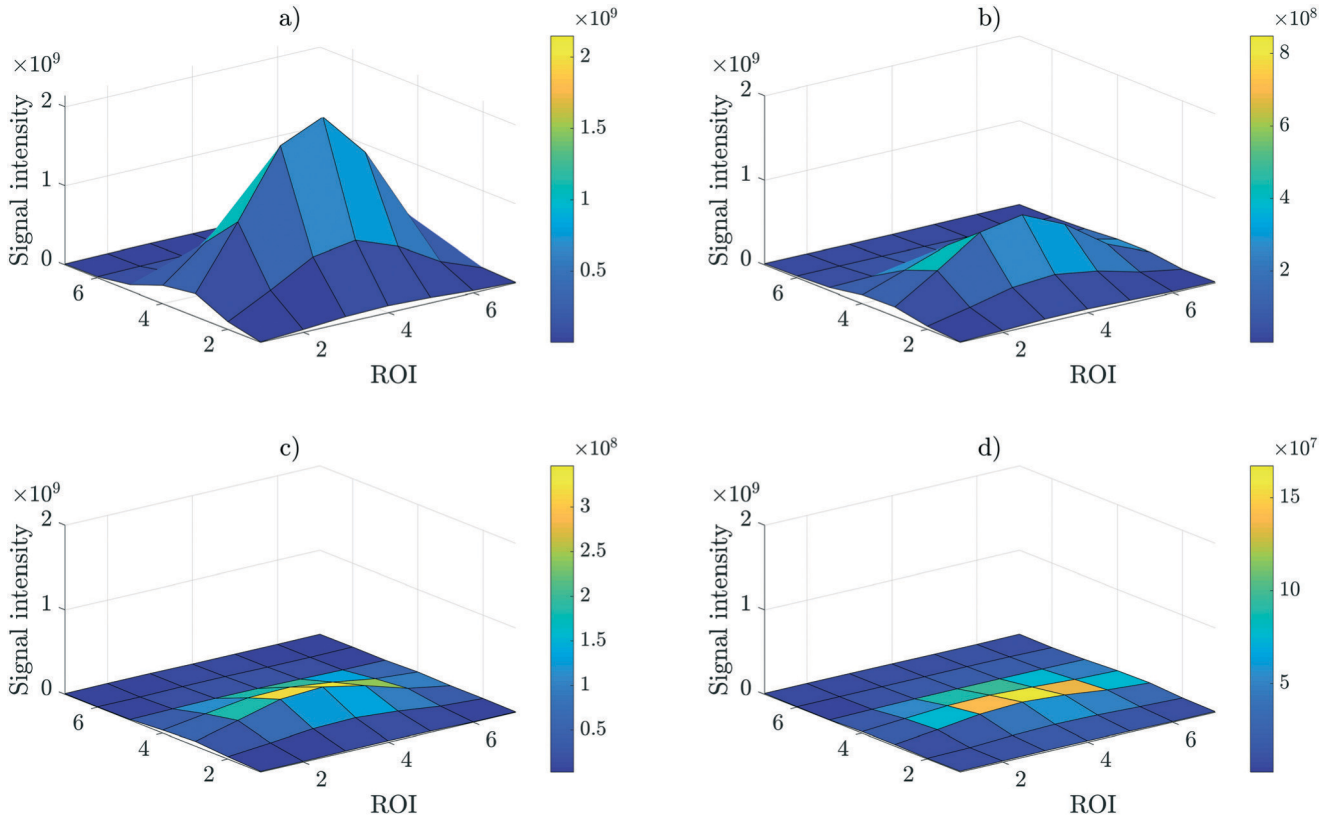

Fig. 4 Signal intensities around the signal maxima for the ethylene glycol thermometer based on the DW-MR images using *b*-values of 50, 2050, 4050, and 6050 s mm^{-2} for a–d, respectively (*cf.*, Fig. 3).

with the experimental values published in the literature. In addition, the results match the prediction from the theory.[27] The observed agreement between experimental data, literature values and theory proves the accuracy of DW-MRI.

4.2.2. Glycerol. The diffusion coefficients obtained in the current study and literature values[26,28,33,34] are plotted in Fig. 6b. The proposed fit of Tomlinson is also shown (eqn (4)) with the fitted curve from the current data (R^2 = 0.99) as solid and dashed lines, respectively. The data measured in the current study shows very good agreement with the literature values and the fitted curve from Tomlinson. The high accuracy obtained in the measurement enables the use of glycerol as a standard NMR thermometer for reactions that occur at a maximum temperature of <290 °C at ambient pressure.

4.2.3. Ionic liquid. The measured diffusion coefficients for the ionic liquid Pyr_{13} [TFSI] are depicted in Fig. 6c. This figure also contains the results of molecular dynamic simulations performed by Lesch *et al.*[35,36] as well as the Vogel–Tammann–Fulcher (VTF) function[37] (eqn (5)) to predict the temperature dependence of the diffusion coefficient. The diffusion coefficients published by Nicotera *et al.* were also added in the figure.[38] The diffusion coefficients measured by DW-MRI match the experimental data from the literature and show a good agreement with the VTF fits (R^2 = 0.98) and MD simulation data. Thus, the chosen ionic liquid is a promising liquid as a NMR thermometer for reactions taking place up to 400 °C, a temperature range that is of great interest for studying reactions such as methanation or Fischer–Tropsch reactions.

4.3. Selection of *b*-values

Since the diffusion weighted signal decays by a factor of exp(−*b*·*D*) and the diffusion coefficients *D* of the three liquids vary from each other, appropriate diffusion weighting (*b*-values) should be applied in order to measure *D* with high precision. An efficient prediction of the optimal diffusion weighting leads to a better design of experiments and thus a shorter total measurement time. In the following, we analyze the use of the different sets of *b*-values for DW-MRI of the three NMR thermometers. In addition, a comparison between the theoretical assumptions and the applied gradient strengths at each temperature point is conducted. To do this, a theoretical assessment was conducted *via* the Cramer–Rao Lower Bound Theory (CRLB)[39] to predict the optimal Δb values for a given diffusion coefficient if four *b*-values and a simple exponential model are used. The CRLB values describe the minimum error of estimated parameters of a model function fitted to experimental data. The results of the analysis are illustrated in Fig. 7a, where the CRLB errors are plotted *versus* the diffusion coefficients for the different Δb values. Basically, with increasing temperature, the desired Δb decreases. This is due to higher diffusivity of the liquids as a result of lower viscosity at higher temperatures. During the measurement, an

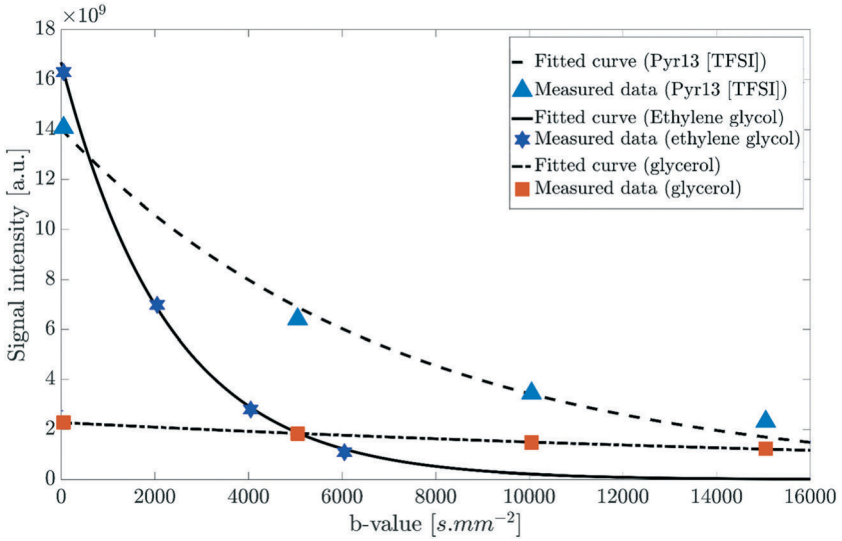

Fig. 5 Signal intensity *versus* *b*-value for Pyr_{13} [TFSI], ethylene glycol, and glycerol measured at 78 °C. The diffusion coefficient can be obtained by fitting the values using eqn (1) ($D_{Pyr13[TFSI]}$ = 1.40 × 10^{-4} mm^2 s^{-1}, $D_{ethylene\ glycol}$ = 4.34 × 10^{-4} mm^2 s^{-1}, and $D_{glycerol}$ = 4.20 × 10^{-5} mm^2 s^{-1}, $R^2 >$ 0.98). Note that a small offset of the curve may occur due to the mean noise level of the image calculated in the magnitude mode. Optimal Δb values were chosen for fitting the data as discussed later in section 4.3.

online analysis of the fitted curves was conducted in order to calculate the fitting error for a specific set of *b*-values. The lowest fitting error was used to determine the optimum diffusion weighting at each temperature. The Δb values applied for the three liquids at different temperatures are illustrated in Fig. 7b. The determined optimal Δb values are in very good agreement with the CRLB predictions. Thus, Fig. 7 gives a straightforward choice of appropriate Δb values in diffusion measurement for the different NMR thermometers.

4.4. General discussion and outlook

The results of the study confirm that the proposed DW-MRI method works very well and can measure the temperature of the catalyst bed. The spatially resolved method enables in-plane measurements of the temperature to provide correct values for boundary conditions in numerical simulations. Three liquids were studied in order to propose three NMR thermometers, which target different temperature ranges for heterogeneously catalyzed reactions.

Comparing the values obtained in the current study and the corresponding data reported in the literature, DW-MRI shows a high accuracy in temperature measurements at elevated temperatures. The reproducibility of this approach has been proven by using different capillaries filled with the same liquids and repeating measurements at certain temperature points three times. The results obtained for the three probing liquids show the broad applicability of the applied method. Which liquid will be the NMR thermometer of choice will depend on the specific applications. Even though ethylene glycol was mainly used for reference temperature measurements by MRSI, DW-MRI of ethylene glycol has proven its value for a temperature range <160 °C, in particular, in case of a low B_0 inhomogeneity. Glycerol with its much lower diffusion coefficients requires strong *b*-values and is thus hardware demanding, particularly at low temperatures. However, glycerol will enable measurements at higher temperatures due to its boiling point of 289 °C and the large changes in *D* for a given temperature difference, leading to more precise results. The ionic liquid exhibits a moderate diffusion coefficient ($D_{ethylene\ glycol} > D_{ionic\ liquid} > D_{glycerol}$). Although the changes in *D* for a given temperature difference are smaller than those for glycerol (*cf.* Fig. 6b and c), the high decomposition temperature makes the ionic liquid a good candidate for temperature measurements up to 400 °C. The automatic analysis of the results is another advantage of the current approach. The automatic analysis not only increases the accuracy of the results, but it also helps to probe the temperature in an arbitrary region of the 3D image as soon as the diffusion weighted images are reconstructed.

The sets of *b*-values applied for the diffusion measurements show that a steady reduction in the chosen Δb is necessary as the temperature increases. The three NMR liquids have different thermodynamic properties, which hindered the optimization of the measurements for a specific liquid used in an NMR thermometer. Therefore, it will be necessary to find an optimal selection of *b*-values for upcoming studies with a certain liquid.

Compared to the promising work published by Koptyug *et al.*, in which the spin–lattice relaxation time T_1 and the signal intensity were used to measure temperature using ^{27}Al MRI in Al_2O_3 samples,[40] the current thermometry by DW-MRI of probing liquids can be applied without using multinuclear NMR hardware. However, since capillaries or capsules have to be inserted into the catalyst support, the proposed approach is not completely non-invasive.

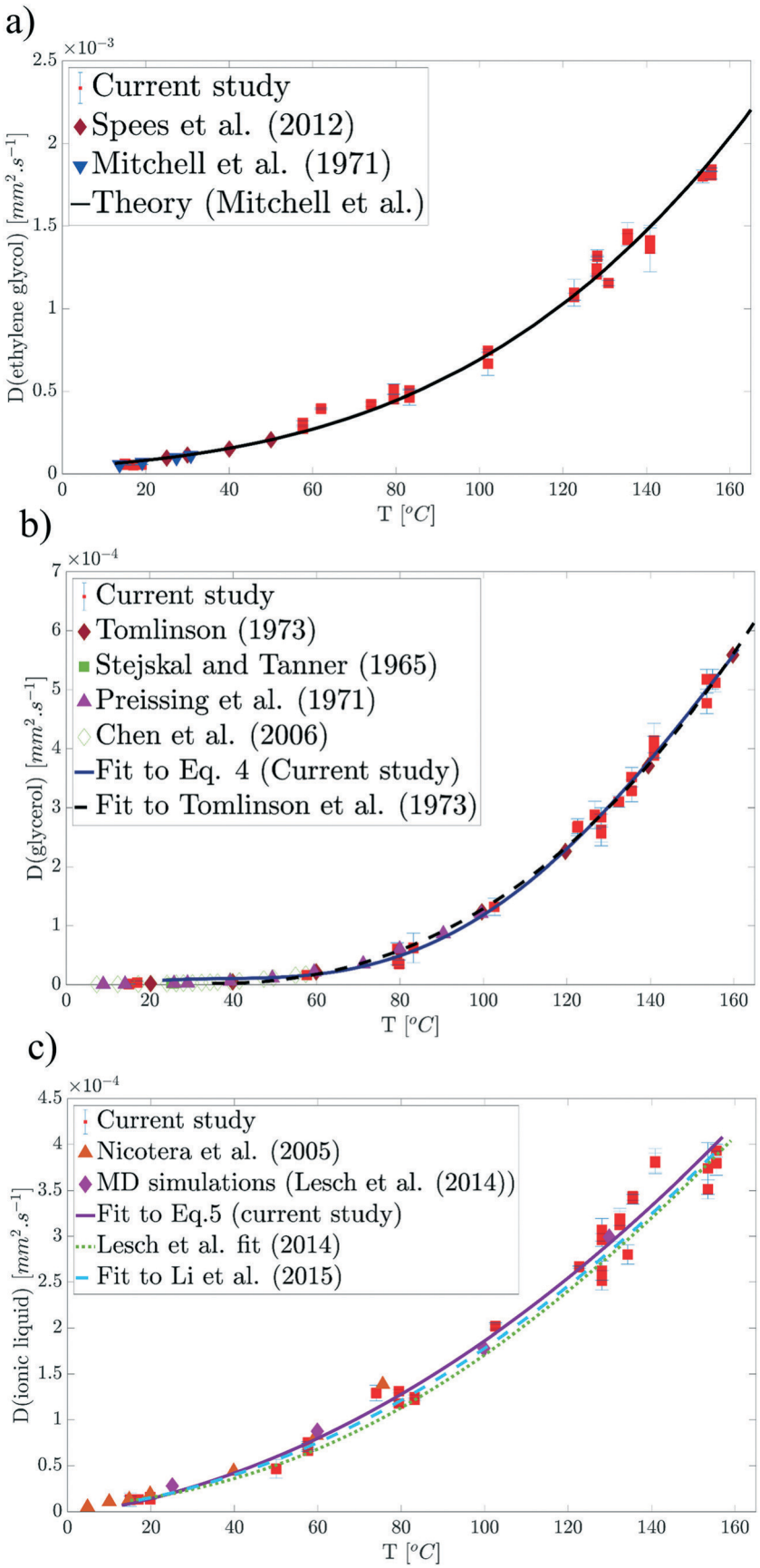

Fig. 6 Diffusion coefficients of a) ethylene glycol, b) glycerol, and c) Pyr_{13} [TFSI] over temperature.

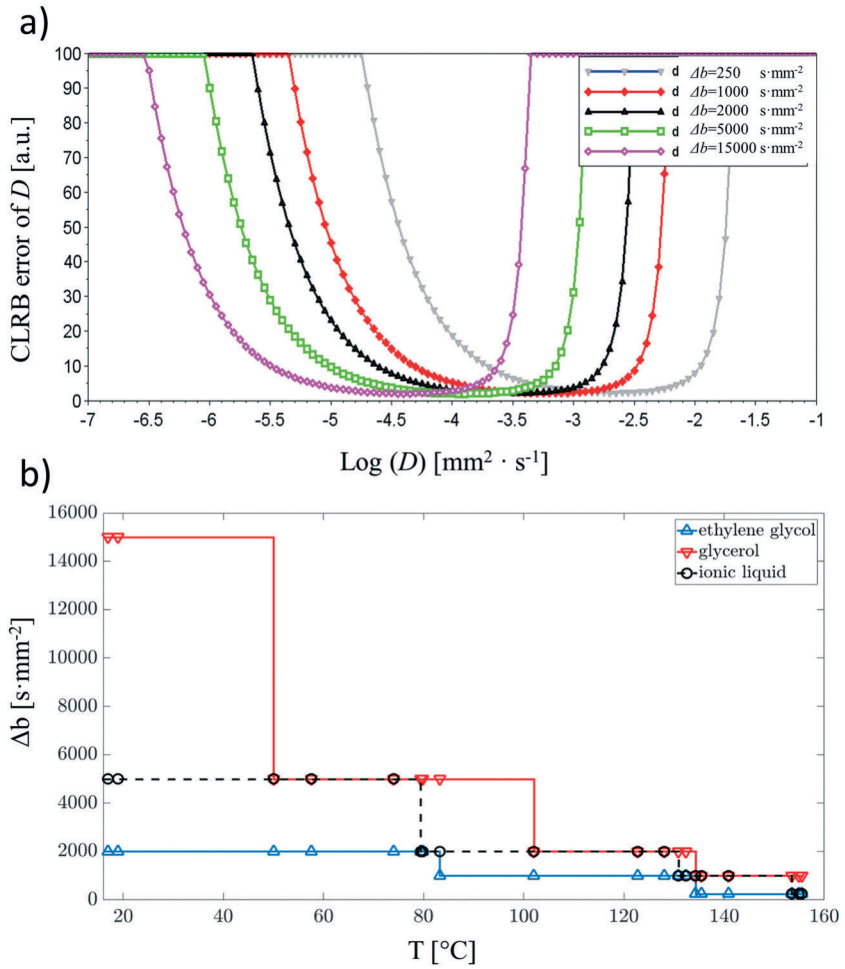

Fig. 7 a) Minimum error of the diffusion coefficient determined from the DW-MRI measurements with four *b*-values plotted *versus* the diffusion coefficient *D*. The error was determined in arbitrary units as Cramer–Rao lower bounds for the different Δb values (diffusion weighting). b) Selection of the optimal Δb out of five applied Δb values for diffusion measurements based on the smallest Cramer–Rao lower bound. The optimal Δb values are depicted *versus* temperature for the three NMR thermometers.

Indisputably, some improvements are necessary to apply the current method as a primary method for temperature measurement of heterogeneous catalysts. For instance, the DW-MRI sequence should be optimized, particularly to reduce the total measurement time and, thus, increase the time resolution of the temperature measurements. Additionally, the number of diffusion weighted experiments and the used *b*-values should be adjusted for a given NMR thermometer and the temperature range of interest.

5. Conclusion

A 3D DW-MRI approach for temperature measurements in heterogeneously catalyzed systems was applied. Using MRSI of ethylene glycol as a reference, the applicability of the method was proven. To be able to increase the feasible temperature range, glycerol and the ionic liquid Pyr_{13} [TFSI] were investigated as temperature stable liquids. In this way, measurements in broad and elevated temperature ranges are possible. The obtained results showed high accuracy and consistency with the literature data. As compared to MRSI, the method is less sensitive to spatial inhomogeneities of the static magnetic field and allows rapid and robust measurements of high temperatures.

Conflicts of interest

There are no conflicts to declare.

Acknowledgements

This work was supported by the German Research Foundation (DFG) in the frame of the Research Training Group GRK 1860 “Micro-, Meso- and Macro-Porous Nonmetallic Materials: Fundamentals and Application” (MIMENIMA), the Federal Ministry for Economic Affairs and Energy (BMWi) and the Federal Ministry of Education and Research (BMBF) in context of the research project “QUARREE 100 - Resilient, integrated and system-friendly energy supply systems in existing urban districts considering the complete integration of renewable energies” (grant number: 03SBE113B).

References

1 M. V. Twigg and J. T. Richardson, *Ind. Eng. Chem. Res.*, 2007, **46**, 4166–4177.
2 L. Kiewidt and J. Thöming, *Chem. Eng. Sci.*, 2015, **132**, 59–71.
3 S. B. Jaffe, *Ind. Eng. Chem. Process Des. Dev.*, 1976, **15**, 410–416.
4 D. Luss and M. Sheintuch, *Catal. Today*, 2005, **105**, 254–274.
5 B. T. Li, K. Maruyama, M. Nurunnabi, K. Kunimori and K. Tomishige, *Ind. Eng. Chem. Res.*, 2005, **44**, 485–494.
6 L. M. Plyasova, T. A. Kriger, A. A. Khassin and A. V. N. Parmon, *Dokl. Phys. Chem.*, 2002, **382**, 47–50.
7 G. M. Carlomagno and G. Cardone, *Exp. Fluids*, 2010, **49**, 1187–1218.
8 L. F. Gladden, F. J. R. Abegão, C. P. Dunckley, D. J. Holland, M. H. Sankey and A. J. Sederman, *Catal. Today*, 2010, **155**, 157–163.
9 A. A. Lysova, A. V. Kulikov, V. N. Parmon, R. Z. Sagdeev and I. V. Koptyug, *Chem. Commun.*, 2012, **48**, 5763–5765.
10 I. V. Koptyug, A. V. Khomichev, A. A. Lysova and R. Z. Sagdeev, *J. Am. Chem. Soc.*, 2008, **130**, 10452–10453.
11 I. V. Koptyug, *Spectrosc. Prop. Inorg. Organomet. Compd.*, 2014, **39**, 1–42.
12 L. F. Gladden, M. D. Mantle and A. J. Sederman, *Adv. Catal.*, 2006, **50**, 1–75.
13 L. F. Gladden and A. J. Sederman, *J. Magn. Reson.*, 2013, **229**, 2–11.
14 J. Ulpts, W. Dreher, L. Kiewidt, M. Schubert and J. Thöming, *Catal. Today*, 2016, **273**, 91–98.
15 J. Ulpts, W. Dreher, M. Klink and J. Thöming, *Appl. Catal., A*, 2015, **502**, 340–349.
16 A. L. van Geet, *Anal. Chem.*, 1968, **40**, 2227–2229.
17 J. Ulpts, L. Kiewidt, W. Dreher and J. Thöming, *Catal. Today*, 2018, **310**, 176–186.
18 H. E. Cline, K. Hynynen, E. Schneider, C. J. Hardy, S. E. Maier, R. D. Watkins and F. A. Jolesz, *Magn. Reson. Med.*, 1996, **35**, 309–315.
19 J. C. Hindman, *J. Chem. Phys.*, 1966, **44**, 4582–4592.
20 D. Le Bihan, J. Delannoy and R. L. Levin, *Radiology*, 1989, **171**, 853–857.
21 Y. Zhang, T. V. Samulski, W. T. Joines, J. Mattiello, R. L. Levin and D. Lebihan, *Int. J. Hyperthermia*, 1992, **8**, 263–274.
22 P. A. Bottomley, T. H. Foster, R. E. Argersinger and L. M. Pfeifer, *Med. Phys.*, 1984, **11**, 425–448.
23 S. Warach, D. Chien, W. Li, M. Ronthal and R. R. Edelman, *Neurology*, 1992, **42**, 1717.
24 M. Iima and D. Le Bihan, *Radiology*, 2016, **278**, 13–32.
25 E. Hahn, *Phys. Rev.*, 1950, **80**, 580–594.
26 E. O. Stejskal and J. E. Tanner, *J. Chem. Phys.*, 1965, **42**, 288–292.
27 R. D. Mitchell, J. W. Moore and R. M. Wellek, *J. Chem. Eng. Data*, 1971, **16**, 57–60.
28 D. J. Tomlinson, *Mol. Phys.*, 1973, **25**, 735–738.
29 D. G. Norris, *Magn. Reson. Med.*, 1991, **17**, 539–542.
30 D. G. Norris, P. Börnert, T. Reese and D. Leibfritz, *Magn. Reson. Med.*, 1992, **27**, 142–164.
31 Y. Y. Lin, P. Hodgkinson, M. Ernst and A. Pines, *J. Magn. Reson.*, 1997, **128**, 30–41.
32 W. M. Spees, S. K. Song, J. R. Garbow, J. J. Neil and J. J. H. Ackerman, *Magn. Reson. Med.*, 2012, **68**, 319–324.
33 G. Preissing, F. Noack, R. Kosfeld and B. Gross, *Z. Phys. Chem.*, 1971, **246**, 84–90.
34 B. Chen, E. E. Sigmund and W. P. Halperin, *Phys. Rev. Lett.*, 2006, **96**, 145502.
35 V. Lesch, S. Jeremias, A. Moretti, S. Passerini, A. Heuer and O. Borodin, *J. Phys. Chem. B*, 2014, **118**, 7367–7375.
36 V. Lesch, Z. Li, D. Bedrov and A. Heuer, *Phys. Chem. Chem. Phys.*, 2016, **18**, 382–392.
37 Z. Li, O. Borodin, G. D. Smith and D. Bedrov, *J. Phys. Chem. B*, 2015, **119**, 3085–3096.
38 I. Nicotera, C. Oliviero, W. A. Henderson, G. B. Appetecchi and S. Passerini, *J. Phys. Chem. B*, 2005, **109**, 22814–22819.
39 O. Brihuega-Moreno, F. P. Heese and L. D. Hall, *Magn. Reson. Med.*, 2003, **50**, 1069–1076.
40 I. V. Koptyug, D. R. Sagdeev, E. Gerkema, H. Van As and R. Z. Sagdeev, *J. Magn. Reson.*, 2005, **175**, 21–29.